Normal and anomalous Doppler effects in a dielectric-loaded stripline cyclotron-resonance maser oscillator

M. Einat and E. Jerby
Faculty of Engineering, Tel Aviv University, Ramat Aviv 69978, Israel
(Received 4 December 1996; revised manuscript received 16 June 1997)

The slow-wave cyclotron-resonance master (CRM) oscillator experiment presented in this paper produces output signals that correspond to normal and anomalous Doppler shifts. The table-top low-voltage (<10 kV) CRM device consists of a double stripline waveguide. The metal strips are loaded by dielectric slabs; thus the waveguide supports slow waves with different phase velocities in odd and even quasi-TEM modes. The suppression of axial electric-field components in this waveguide eliminates the Cherenkov interaction as a parasitic effect to the slow-wave CRM. Oscillations are observed in the frequency range 3–15 GHz. Doppler shifts of 30% down and 150% up are measured with respect to the electron cyclotron frequency. These agree with the normal and anomalous tuning conditions, respectively. The dielectric-loaded stripline scheme is discussed for practical slow-wave CRM devices. [S1063-651X(97)09010-7]

PACS number(s): 41.60.−m, 84.40.Ik

I. INTRODUCTION

The cyclotron-resonance maser (CRM) interaction [1] takes place between a guided electromagnetic wave and a rotating electron beam in an axial magnetic field. It satisfies the tuning condition

$$\omega = n\omega_c \pm k_z V_{ez}, \tag{1}$$

where ω and k_z are the wave angular frequency and axial wave number, respectively. The electron cyclotron frequency is $\omega_c = eB_0/\gamma m$, where B_0 is the axial magnetic field and e, m, γ, and V_{ez} are the electron charge, mass, relativistic factor, and axial velocity, respectively. The integer n denotes the order of the cyclotron harmonic interacting with the electromagnetic (em) wave.

CRM devices and gyrotrons [2] are operated typically with *fast* em waves in hollow metallic tubes where the axial phase-velocity component is larger than the speed of light $V_{\rm ph} = \omega/k_z > c$. CRM-type interactions are possible as well with *slow* waves $V_{\rm ph} < c$ in dielectric-loaded or periodically loaded waveguides [3–20].

The *anomalous* Doppler effect [3–5] occurs when the em wave is slower than the electron beam, i.e., $V_{\rm ph} < V_{ez}$. The Doppler shift is larger than the cyclotron frequency and consequently the CRM interaction is possible only with a *negative* cyclotron harmonic $n \leqslant -1$. Tuning diagrams of normal and anomalous CRM interactions are illustrated for comparison in Figs. 1(a) and 1(b). The diagrams show the em-wave dispersion line and the electron-beam line given by Eq. (1). Figure 1(a) shows the normal operating regime, where points A and B denote CRM interactions with backward and forward waves, respectively. The Doppler shift is positive for a forward wave and negative for a backward wave. The CRM interaction in the anomalous regime [Fig. 1(b)] takes place with a negative cyclotron harmonic and a forward slow wave.

Experimental indications for the anomalous Doppler effect were reported in metallic periodic waveguide [3,4] and in dielectric-loaded waveguide [5] experiments. Other studies related to this subject are the slow-wave CRM amplifier experiment (conducted in the normal regime $V_{ez} < V_{\rm ph} < c$)[6] and the dielectric-loaded cyclotron autoresonance maser (CARM) experiment [7]. Periodic waveguides made of arrays of metal posts were used as artificial dielectrics in CRM experiments [18–20]. A quasianomalous effect in a periodic-waveguide CRM is proposed in Ref. [21].

The advantages of the slow-wave CRM interaction, compared to the fast-wave device, are: (a) an alleviation of the initial electron rotation, (b) a larger Doppler shift, and (c) a wider spectral bandwidth. On the other hand, the difficulties in using dielectric-loaded CRMs stem from the vicinity between the dielectric and the electron beam, which may cause charging effects and possibly damage to the dielectric material.

This paper presents a CRM experiment in a double-stripline waveguide. The metallic strips stretched along the tube are loaded by dielectric slabs. They support quasi-TEM modes in a wide spectral bandwidth and protect the dielectric slabs from the electron beam. This slow-wave CRM device yields anomalous and normal operating modes, without a disturbing Cerenkov interaction, which might appear as a parasitic effect in other slow-wave CRM schemes [12] (this effect is suppressed here by the absence of axial electric-field components in the waveguide). The table-top CRM setup and the experimental results are described in the following sections.

II. EXPERIMENTAL SETUP

The dielectric-loaded CRM oscillator experiment presented in this paper operates at low accelerating voltages (<10 kV). The electron beam, generated by a thermionic Pierce gun, is injected into a waveguide tube where it is confined and spun by a solenoid. The axial magnetic field on the cathode is 0.6 of its value in the interaction region. The electron beam is dumped at the exit of the interaction region onto a collector, which is also used to measure the electron

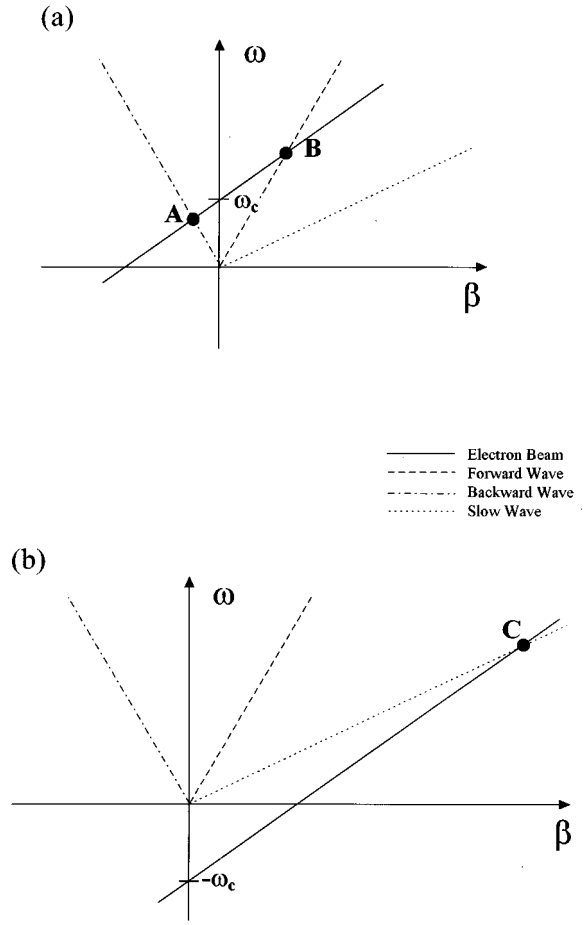

FIG. 1. Tuning diagrams of CRM interactions: (a) normal Doppler interactions with backward (A) and forward (B)waves and (b) an anomalous Doppler effect with a slow forward wave (C) for which $V_{\rm ph}<V_{ez}$.

current. Approximately 0.4 of the total cathode current is scraped, mostly by the anode. Two synchronized pulsers generate the solenoid and the electron gun pulses, as described in Ref. [20]. The experimental parameters are listed in Table I.

The double-stripline dielectric-loaded waveguide used in this experiment is shown in Fig. 2. Two copper strips are attached to dielectric slabs stretched along the sidewalls of a standard WR90 rectangular metallic tube. The dielectric slabs are made of a commercial ceramic (MCT-140 of Trans-Tech Ceramics Inc.) with a high dielectric constant $\varepsilon_r=140$. The metal strips serve both a mechanical and an electrical function. First, they protect the dielectric slabs from the electron beam, thus preventing them from being electrically charged and damaged. Second, they support even and odd quasi-TEM transverse modes. The cavity formed by two mirrors with holes at both ends of the waveguide determines the axial modes for the CRM oscillator.

The transverse electric-field profiles of the odd and even quasi-TEM modes are illustrated in Fig. 3. These modes have a zero cutoff frequency and consequently they enable a wideband tunability of the CRM oscillator. On the other hand, the dielectric loading reduces the coupling between the em wave and the electron beam. Double-stripline waveguides have been used also in our free-electron maser

TABLE I. Experimental parameters.

Electron beam	
energy (keV)	<10
current (A)	<0.5
pulse width (ms)	~1
electron-beam diameter (mm)	5
Magnetic field	
uniform solenoid (kG)	1–3
Waveguide	
rectangular tube (in.^{2})	0.9×0.4
gap between striplines (mm)	11
resonator length (cm)	49
dielectric slabs:	
dielectric constant	140±10%
cross section (in.^{2})	0.2×0.4
frequency range (GHz)	3–15

experiments with and without dielectric loading (Refs. [22] and [23], respectively). The dielectric-loaded waveguide shown in Fig. 2 resemble two *microstrip* guides in a back-to-back coupling (planar microstrips are well-known waveguides in the microwave integrated-circuit technology [24]). The different transverse field profiles of the odd and even quasi-TEM modes result in different effective dielectric loading and phase velocity for each mode. The effective dielectric constants $\varepsilon_{\rm eff}$ were measured by a vector-network analyzer [Hewlett Packard (HP) 8720A] in the time domain. The results presented in Ref. [22] are $\varepsilon_{\rm eff}\sim 8$ and ~ 140 for the odd and even modes, respectively.

The CRM tuning relation (1) for the nondispersive quasi-TEM mode is

$$\omega=\frac{n\omega_c}{1\mp\sqrt{\varepsilon_{\rm eff}}\beta_{ez}}, \tag{2}$$

where $\beta_{ez}=V_{ez}/c$ and the minus and plus signs correspond to forward and backwards waves, respectively. Hence the resulting condition for the anomalous interaction with a forward wave is $\sqrt{\varepsilon_{\rm eff}}\beta_{ez}>1$. This condition can be satisfied in our experiment by the even quasi-TEM mode ($\varepsilon_{\rm eff}\cong 140$, $\beta_{ez}=0.15$), with off-axis or large orbit electrons.

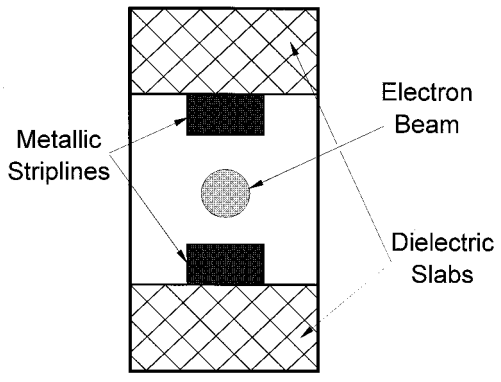

FIG. 2. Dielectric-loaded double-stripline waveguide.

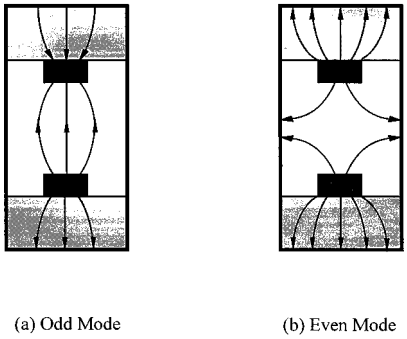

FIG. 3. Illustrations of the transverse electric-field profiles of the (a) odd and (b) even quasi-TEM modes.

The diagnostic setup is shown in Fig. 4. The spectral evolution of the CRM output is measured simultaneously with the electron-gun voltage, collector current, an solenoid field. The em wave evolved in the cavity is sampled by a small rf probe and is split into two arms; one for a direct detection of the envelop by a crystal detector (HP 8474D) and the other for a heterodyne analysis. The latter consists of a mixer (HP 5364A), a local oscillator (HP 83752A), and a frequency-time domain analyzer (HP 5372A), which measures the temporal evolution of the signal frequency during the pulse.

III. EXPERIMENTAL RESULTS

Oscillations are observed in this experiment in the frequency range 3–15 GHz. Doppler shifts of 30% down and 150% up measured with respect to the electron cyclotron frequency. The rf power coupled out for the CRM in this experiment is within the range 1–10 W. This sampling level is sufficient for the spectral measurements aimed in this study.

Two types of signals, related to the normal and the anomalous regimes, are observed in different launching conditions of the electrons into the interaction region. The first signal type, which appears when the electrons are launched off axis into the interaction region is presented in Figs. 5(a)–5(c). The sweep in the electron-gun voltage during the pulse is shown in Fig. 5(a). The corresponding burst of rf radiation is shown in Fig. 5(b). It takes place in an electron energy sweep from 9 to 5 keV. The temporal evolution of the frequency along this pulse is shown in Fig. 5(c). The em-wave frequency is slightly increased near 5.3 GHz. The cyclotron frequency in this run is $f_c = eB_0/2\pi\gamma m = 8\,\mathrm{GHz}$. According to Eq. (1), this Doppler downshift (~30%) corresponds to a

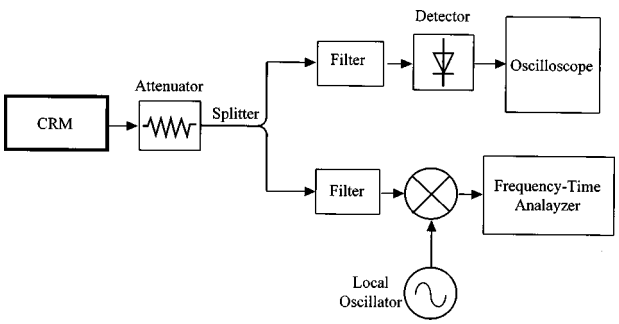

FIG. 4. Diagnostic setup.

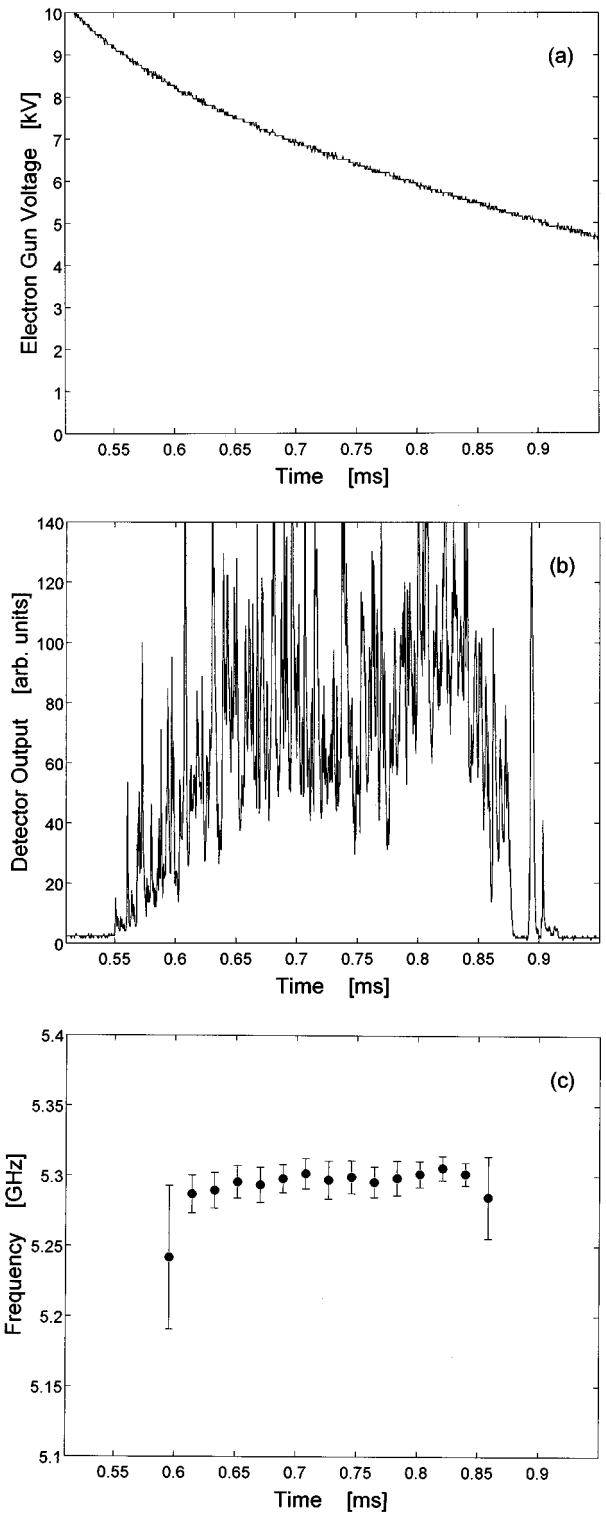

FIG. 5. Measurements of a normal CRM interaction ($f_c = 8$ GHz): (a) electron gun voltage, (b) detector output, and (c) frequency-time domain measurements.

normal backward-wave interaction with the odd quasi-TEM mode ($\varepsilon_{\mathrm{eff}} = 8$), as shown schematically by point *A* in Fig. 1(a). The electron pitch angle is estimated by a trajectory simulation to be $\alpha = V_\perp / V_\parallel \sim 0.2$ in this case.

The other type of interaction, observed by launching the

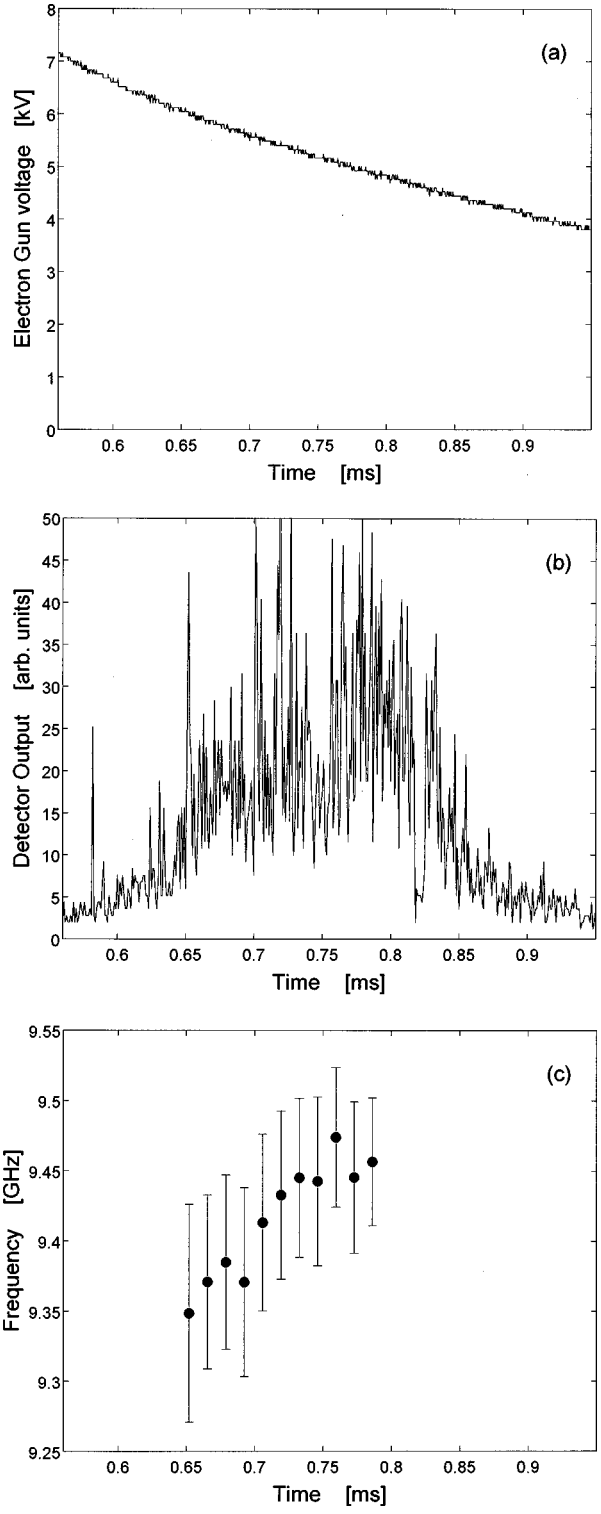

FIG. 6. Measurements of a anomalous CRM interaction ($f_c = 3.7$ GHz): (a) electron gun voltage, (b) detector output, and (c) frequency-time domain measurements.

electrons on axis, is presented in Figs. 6(a)–6(c). The electron-gun voltage sweep and the corresponding rf output burst are shown in Figs. 6(a) and 6(b), respectively. The frequency variation during the pulse, measured by the frequency-time domain analyzer, is shown in Fig. 6(c). The experimental results show that, in this operating regime, the

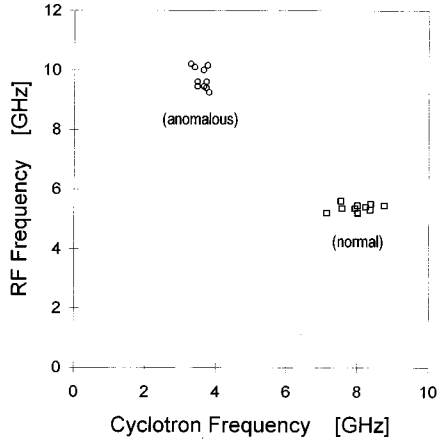

FIG. 7. Accumulation of the radiation frequency vs the cyclotron frequency in different experimental runs. The two groups show the normal and anomalous regimes.

frequency increases when the electron energy decreases. The cyclotron frequency in this CRM operating mode is $f_c = 3.7$ GHz, whereas the em-wave frequency varies from 9.35 to 9.47 GHz during the pulse. According to Eq. (1), this signal corresponds to an *anomalous* interaction of the negative second cyclotron harmonic ($n = -2$) with the even quasi-TEM mode ($\varepsilon_{\text{eff}} \approx 140$). This operating mode is shown schematically in Fig. 1(b). These experimental results introduce a frequency upshift of 150% with respect to the cyclotron frequency. The electron pitch angle is estimated in this case to be $\alpha = V_\perp / V_\parallel \sim 0.02$.

The normal and anomalous operating regimes are demonstrated by an accumulation of experimental results in Fig. 7. It shows the radiation frequency vs the cyclotron frequency in 20 experimental runs. The two groups correspond to the normal and anomalous operating modes, as presented above. Figure 7 show the typical spread of the results from shot to shot in these two CRM modes. The corresponding synchronism diagrams of these operating modes in our experiment are shown schematically in Fig. 8, where the dispersion lines of the odd and even waveguide modes (without the electron beam) are deduced from the time-delay measurements presented in Ref. [22].

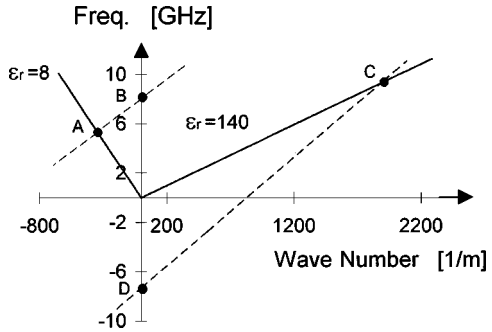

FIG. 8. Synchronism diagrams for the normal and anomalous regimes presented in Fig. 7. The solid liens illustrate the waveguide dispersions in the odd and even modes ($\varepsilon_{\text{eff}} = 8$ and 140, respectively [22]), the dashed lines show the electron-beam lines [Eq. (1)], the intersection points *A* and *C* denote the two CRM interactions, and points *B* and *D* show the corresponding cyclotron frequencies.

IV. DISCUSSION

The normal and anomalous CRM interactions are demonstrated in a dielectric-loaded stripline waveguide that supports slow quasi-TEM modes. The anomalous CRM concept provides a wide-band tunability without an initial rotation of the beam, as demonstrated in our experiment. The metallic strips protect the dielectric loading from the electron beam and alleviates a technical difficulty in using dielectrics in CRM tubes. The use of a low-energy electron beam ($\gamma \sim 1.02$) decreases the relativistic effect, which reduces the cyclotron frequency in relativistic CRM devices. Consequently, the net frequency upshift observed is relatively large and is comparable to that obtained in an advanced CARM experiment reported recently [25].

The different rates of the frequency sweeps shown in Figs. 5(c) and 6(c) support the interpretation of the two different types of signals observed, as normal and anomalous CRM interactions, respectively. The derivative of Eq. (2) results in

$$\frac{d\omega}{d\beta_{ez}} = \pm \sqrt{\varepsilon_{\text{eff}}}\,\frac{\omega^2}{n\omega_c}. \tag{3}$$

Hence the frequency sweep rate of the anomalous interaction with a forward even mode is negative ($n=-2$) and is much larger than the (negative) sweep rate of the normal interaction with a backward odd mode. This difference between the two operating modes of the slow-wave CRM is clearly observed in the experiment.

Using the present experimental parameters, Eq. (3) shows that the frequency sweep rate in the anomalous CRM mode is larger by more than an order of magnitude than that in the normal operating mode ($d\omega/d\beta_{ez}=-9\times10^{11}$ s^{-1}compared to -6×10^{10}s^{-1}, respectively). A similar ratio between the two sweep rates is observed in the experiment, but the experimental sweep measurements in both CRM modes ($d\omega/d\beta_{ez}=-7\times10^{10}$ s^{-1}and -4×10^{9} s^{-1}, respectively) are smaller than those results from Eq. (3). This difference might be attributed to the finite bandwidth of the CRM interaction and to mechanisms of mode competition in the cavity.

The large spikes observed in Figs. 5(b) and 6(b) always appear in this experiment. These might be related to hopping between axial modes in the cavity, but their resemblance to the spikes observed in a free-electron laser oscillator experiment [26] may relate them to a self-mode-locking mechanisms. This effect, as well as other related to this CRM scheme, will be studied in future experimental and theoretical studies.

The rf extraction efficiency has not been measured in the present spectral analysis study. The dialectic-loaded CRM efficiency is proportional to $1/\sqrt{\varepsilon_{\text{eff}}}$ and therefore is much smaller than the high efficiency observed in gyrotron and CARM experiments [25]. However, the dielectric-loaded stripline scheme provides a simple way to taper the waveguide parameters by varying the width of the metal strip along the tube. Thus the phase velocity and impedance can be tailored along the waveguide in order to satisfy, locally, the optimal conditions for the slow-wave CRM interaction. This efficiency-enhancement scheme for stripline CRMs is a subject for future study.

In addition to the scientific interest, the table-top CRM demonstrated in this experiment may lead to the development of a practical device for useful applications. In particular, miniature CRM devices can be conceived in a technology of microwave integrated circuits based on microstrip lines.

ACKNOWLEDGMENT

This research was supported in part by the Israeli Academy of Science and Humanities, and the Israeli Ministry of Energy.

[1] J. L. Hirshfield and V. L. Granatstein, IEEE Trans. Microwave Theory Tech. **MTT-25**, 522 (1977), and references therein.
[2] V. A. Flyagin, A. V. Gaponov, M. I. Petelin, and V. K. Yulpatov, IEEE Trans. Microwave Theory Tech. **MTT-25**, 514 (1977).
[3] B. I. Ivanov, D. V. Gorozhanin, and V. A. Miroshnichenko, Pis'ma Zh. Tekh. Fiz. **5**, 1112 (1979) [Sov. Tech. Phys. Lett. **5**, 464 (1979)].
[4] S. Y. Galuzo, V. L. Slepkov, and V. A. Pletyushkin, Zh. Tekh. Fiz. **52**, 1681 (1982) [Sov. Phys. Tech. Phys. **27**, 1030 (1982)].
[5] A. N. Didenko, A. R. Borisov, G. P. Fomenko, and A. S. Y. G. Shtein, Pis'ma Zh. Tekh. Fiz. **9**, 1331 (1983) [Sov. Tech. Phys. Lett. **9**, 572 (1983)].
[6] H. Guo, L. Chen, H. Keren, J. L. Hirshfield, S. Y. Park, and K. R. Chu, Phys. Rev. Lett. **49**, 730 (1982).
[7] K. C. Leou, D. B. McDermott, and N. C. Luhmann, Jr. (unpublished).
[8] V. K. Jain, V. K. Tripathi, and R. K. Patnaik, IEEE Trans. Plasma Sci. **PS-14**, 31 (1986).
[9] T. H. Kho and A. T. Lin, Phys. Rev. A **38**, 2883 (1988).
[10] D. B. McDermott, H. Cao, and N. C. Luhmann, Int. J. Electron. **65**, 477 (1988).
[11] A. K. Ganguly and S. Ahn, Phys. Rev. A **42**, 3544 (1990).
[12] T. H. Kho and A. T. Lin, IEEE Trans. Plasma Sci. **18**, 513 (1990).
[13] J. L. Vomvoridis and C. T. Iatrou, Int. J. Electron. **71**, 145 (1991).
[14] C. T. Iatrou and J. L. Vomvoridis, Int. J. Electron. **71**, 493 (1991).
[15] K. C. Leou, D. B. McDermott, and N. C. Luhman, Jr., IEEE Trans. Plasma Sci. **20**, 188 (1992).
[16] Y. H. Cho, D. I. Choi, and J. S. Choi, Opt. Commun. **101**, 100 (1993).
[17] Y. Z. Yin, Int. J. Infrared Millim. Waves **14**, 1587 (1993).
[18] E. Jerby and G. Bekefi, Phys. Rev. E **48**, 4637 (1993).
[19] E. Jerby, Phys. Rev. E **49**, 4487 (1994).
[20] E. Jerby, A. Shahadi, V. Grinberg, V. Dikhtiar, M. Sheinin, E. Agmon, H. Golombek, V. Trebich, M. Bensal, and G. Bekefi, IEEE J. Quantum Electron. **31**, 970 (1995).
[21] M. Korol and E. Jerby, Nucl. Instrum. Methods Phys. Res. A **375**, 222 (1996).

[22] M. Einat, E. Jerby, and A. Shahadi, Nucl. Instrum. Methods Phys. Res. A **375**, 21 (1996).

[23] R. Drori, E. Jerby, and A. Shahadi, Nucl. Instrum. Methods Phys. Res. A **358**, 151 (1995).

[24] B. C. Wadell, *Transmission Line Design Handbook* (Artech House, London, 1991).

[25] V. L. Bratman, G. G. Denisov, B. D. Kol'chugin, S. V. Samsonov, and A. B. Volkov, Phys. Rev. Lett. **75**, 3102 (1995).

[26] E. Jerby, G. Bekefi, and J. C. Wurtele, Phys. Rev. Lett. **66**, 2068 (1991); IEEE J. Quantum Electron. **27**, 2512 (1991).